

## Preparation of Nanocellulose *via* Transition Metal Salt-Catalyzed Hydrolysis Pathway

Mazlita Yahya, Hwei Voon Lee,\* and Sharifah Bee Abd Hamid

Nanocellulose was successfully prepared from microcrystalline cellulose (MCC) *via* nickel salt-catalyzed hydrolysis under mild reaction conditions of 45 °C for 15 min. The mild acid nickel salt-catalyzed hydrolysis was able to selectively depolymerize the amorphous regions of cellulose and retain its crystalline region, thus improving the crystallinity of the treated product at the nanoscale up to 80%. FTIR analysis confirmed that the basic cellulose structure of inorganic metal salt-treated products was maintained and that no derivative was formed. Furthermore, the synthesized Ni-treated nanocellulose (NTC) products appeared in the form of cluster fragments with spider-web-like appearance (fiber diameter of 10 to 60 nm and fiber length of 300 to 600 nm), thus providing aspect ratios in the range of 7.96 to 9.11. In addition, NTC products exhibited relatively higher thermal stability as compared to MCC because of the presence of high crystallinity phases and the absence of impurities (such as nitrate ions) on the nanocellulose surface. Thus, the present study concluded that nickel-based inorganic salt is an efficient and selective catalyst for the hydrolysis of MCC with high simplicity in operation and short preparation time.

*Keywords:* Cellulose nanocrystal; Depolymerization; Lignocellulosic biomass; Acid hydrolysis; Nanocellulose

*Contact information:* Nanotechnology & Catalysis Research Centre (NANOCAT), 3rd Floor, Block A, Institute of Postgraduate Studies (IPS), University of Malaya, 50603 Kuala Lumpur, Malaysia;

\* *Corresponding author:* leehweivoon@um.edu.my

### INTRODUCTION

Nanocellulose (NC) is a new class of biopolymer of nanoscale dimensions that is creating a revolution in biobased-materials for various industrial applications, such as personal care, chemical, foods, pharmaceuticals, and bio-composites. It is equipped with unique nanoscale characteristics, including high reinforcing strength and stiffness (comparable to Kevlar and steel), high surface area, unique optical properties, and hydrophilic/hydrophobic properties. Unlike other lightweight, high strength materials derived from fossil fuels, nanocellulose is biodegradable and renewable, making it a promising green alternative for further exploration by both research scientist and industry (Himmel *et al.* 2007; Lange 2007).

NC is prepared from inexpensive renewable lignocellulosic biomass (LCB), which consists of a large percentage of cellulose (40% to 50%), hemicellulose (20% to 30%), and lignin (0 to 20%). It can be generated as rod-like nanocrystalline cellulose (CNC) or longer cellulose nanofibrils (CNFs) from plant cell walls (Peng *et al.* 2011). Generally, nanopolymeric cellulose can be isolated *via* biological hydrolysis (enzyme) or chemical acid hydrolysis (strong acid) of the glycosidic bonds of cellulose fibers (Brinchi *et al.* 2013). However, isolation techniques are still problematic because of the presence of strong intra- and intermolecular hydrogen bonding and van der Waals forces linking the

cellulose fiber network. This highly organized bonding can create a defensive barrier to protect the plant structure (Lindman *et al.* 2010). The enzymatic hydrolysis of lignocellulosic materials requires several days to digest the structural barriers before the hydrolysis process. In the case of strong acid treatment, hydronium ions can efficiently break down or attack intermolecular and intramolecular bonds in cellulose. This treatment is more effective in comparison to enzymatic treatment. However, the use of a strong acid is usually accompanied by over-degradation of cellulose and has drawbacks such as equipment corrosion. Thus, diluted or organic acids have been suggested for milder reactions, but such treatments have been found to be less effective in reacting to the plant's structure (Lee *et al.* 2014).

Inorganic salts in the categories of trivalent ( $\text{FeCl}_3$ ,  $\text{Fe}_2(\text{SO}_4)_3$ ,  $\text{Al}(\text{NO}_3)_3$ ), divalent ( $\text{CaCl}_2$ ,  $\text{FeCl}_2$ ,  $\text{FeSO}_4$ ), and monovalent ( $\text{NaCl}$ ,  $\text{KCl}$ ) have been considered by others as potential catalysts for hydrolysis treatment for several purposes: i) degradation of hemicellulose and cellulose in biomass (Liu *et al.* 2009; Zhao *et al.* 2011; Kamireddy *et al.* 2013; López-Linares *et al.* 2013); ii) conversion of cellulose to glucose (Zhang *et al.* 2015); and iii) extraction of micro- or nano-crystalline cellulose (Hamid *et al.* 2014; Lu *et al.* 2014; Li *et al.* 2015). It has been reported that the valence state of metal ion is the key factor to influence the hydrolysis efficiency, where acidic solution ( $\text{H}^+$ ) was generated during polarization between metal ions with water molecules (Kamireddy *et al.* 2013). A higher valence state will generate more  $\text{H}^+$  ions, which act effectively in the co-catalyzed acid hydrolysis reaction in the presence of metal ion.

At present, acid hydrolysis of cellulose is still considered to be the most efficient pathway for high-yield nanocellulose production. To achieve a technically feasible, selective, and controllable hydrolysis process, a transition metal-based catalyst can be used because of its mild acidity. Transition metal-based catalysts, such as an iron-based catalyst, were found to contain Lewis acid sites and can perform the hydrolysis of cellulose efficiently (Lee *et al.* 2014). Several studies have reported the use of iron-based inorganic salts (*e.g.*,  $\text{FeCl}_3$ ) for hydrolysis of cellulose into nanocellulose. These research findings indicate that  $\text{Fe}^{3+}$  from the  $\text{FeCl}_3$ -catalyzed hydrolysis can selectively diffuse into the amorphous regions of cellulose and promote the cleavage of glycosidic linkages of cellulose chains into smaller dimensions. Furthermore, the presence of an acidic medium (HCl) or ultrasonic-assisted treatment can act synergistically to improve the accessibility of metal ions for the hydrolysis process (Karim *et al.* 2014; Lu *et al.* 2014; Li *et al.* 2015).

In this study, a nickel-based inorganic salt with divalent ( $\text{Ni}^{2+}$ ) was selected as a hydrolysis catalyst for the selective depolymerisation of a cellulose model compound (microcrystalline cellulose, MCC) into nanocellulose. The Ni-catalyst contained both acidic and metallic active sites, which actively promote simultaneous hydrolysis and hydrogenation process. Yang's research group successfully converted microcrystalline cellulose into sorbitol by nickel phosphides catalyst (Yang *et al.* 2012). Furthermore, He *et al.* (2012) reported the use of Ni-catalyst for selective cleavage of 4-O-5 ether bond (C-O) of aromatic ethers (diphenyl ether) *via* hydrolysis process to phenol product, verifying that the Ni center is the active site for C-O bond cleavage (He *et al.* 2012). To the best of our knowledge, no study had yet been conducted to investigate the preparation of nanocellulose *via* the Ni-salt hydrolysis pathway. The Ni-salt with various acid concentrations was prepared to study the efficiency of selective acid hydrolysis of the amorphous regions while retaining the crystalline regions of cellulose. Furthermore, physicochemical properties and structural changes of MCC and Ni-treated product were subsequently investigated.

## EXPERIMENTAL

### Materials

The cellulose model compound used was microcrystalline cellulose (MCC, Sigma-Aldrich, USA). The chemical reagents used were nickel (II) nitrate hexahydrate ( $\text{Ni}(\text{NO}_3)_2 \cdot 6\text{H}_2\text{O}$ , System, Malaysia).

### Methods

#### *Preparation of nanocellulose*

Microcrystalline cellulose (MCC) was added to prepare Ni-salt solutions with various concentrations (0.05, 0.5, and 1.0 M) at 45 °C, and the solution was stirred for 15 min. The pH values of the Ni-salt solutions at 0.05, 0.5, and 1.0 M were 6.3, 5.4, and 5.0, respectively. After hydrolysis, the treated product was repeatedly washed with deionized water until the medium reached neutrality (pH 7). Subsequently, the gelatinous product was dialyzed using a dialysis tube to completely remove the residue of  $\text{Ni}^{2+}$  or  $\text{NO}_3^-$  ions attached to the surface of the product. The slurry was further treated with 40 kHz sonication for 40 min in a sonicator (WUC-A03H, DAIHAN, Korea) to disperse the nanofibers in water. Finally, the products were dried in a freeze dryer to obtain a fine white powder. The Ni-treated nanocellulose synthesized at Ni-salt concentrations of 0.05, 0.5, and 1.0 M was denoted NTC0.05, NTC0.5, and NTC1.0, respectively.

#### *Characterization*

X-ray diffraction (XRD) patterns of the raw material (MCC), NTC0.05, NTC0.5, and NTC1.0 were obtained within a  $2\theta$  range from 5 to 40° using a Shimadzu (Japan) diffractometer model XRD 6000, with  $\text{CuK}\alpha$  radiation at an operating voltage of 2.7 kW. The crystallinity index (CrI) of samples was calculated based on the intensity between the (002) and (101) lattice diffraction peaks using Segal's method (Segal *et al.* 1959) (Eq. 1). In this equation  $I_{002}$  represents both crystalline and amorphous region of cellulose (maximum intensity at  $2\theta = 22^\circ$ ), while  $I_{\text{am}}$  represents only the amorphous phase (intensity of diffraction at  $2\theta = 18^\circ$ ):

$$\text{CrI} (\%) = \frac{I_{002} - I_{\text{am}}}{I_{002}} \times 100\% \quad (1)$$

The crystallite size was calculated based on the full width at half maximum (FWHM) of 002 reflections, which is by using Debye-Scherrer's equation (Eq. 2),

$$D = \frac{0.9\lambda}{\beta_{hkl} \cos \theta_{hkl}} \quad (2)$$

where  $D$  is the crystallite size for the (hkl) phase (nm),  $\lambda$  is the X-ray wavelength of radiation for  $\text{CuK}\alpha$  (0.154 nm),  $\beta_{hkl}$  is the full width at half maximum (FWHM) at (hkl) peak, and  $\theta$  is the diffraction angle for the (hkl) phase. Generally, the strongest peak appeared at the XRD plane of 002, and this was selected for the measurement of crystallinity index and crystallite size.

Fourier transform infrared spectroscopy (FTIR) was performed using a Perkin Elmer (USA) spectrometer (Spectrum Two) in the range of 4000 to 500  $\text{cm}^{-1}$  with a

scanning resolution of  $4 \text{ cm}^{-1}$ . Ground samples were mixed with potassium bromide (KBr) and then pressed into ultra-thin transparent pellets for analysis.

The dimensions of hydrolyzed celluloses (NTC0.05, NTC0.5, and NTC1.0) were determined using high-resolution transmission electron microscopy (HRTEM) analysis (JEOL JEM-2100F, USA) at an acceleration voltage of 200 kV. NFC samples diluted in ethanol ( $\text{C}_2\text{H}_5\text{OH}$ ) were deposited on the surface of copper grids and allowed to dry at room temperature. Aspect ratios in terms of length to diameter (L/D) of treated samples (NTC0.05, NTC0.5, and NTC1.0) were determined based on the TEM measurement.

The surface morphology of the raw material (MCC) and treated samples were studied using field-emission scanning electron microscopy (FESEM; FEI Quanta 200F, USA) operating at 10 kV and 100 Pa, *i.e.*, low-vacuum conditions. The samples were mounted with conductive carbon tape and coated with 5 nm of gold before FESEM imaging.

Thermal analysis was performed using a thermogravimetric analyzer (TGA) Q-500 (TA Instruments, USA). One milligram of each sample was heated at  $10 \text{ }^\circ\text{C}/\text{min}$  from 25 to  $900 \text{ }^\circ\text{C}$  under nitrogen ( $\text{N}_2$ ) gas at a flow rate of 200 mL/min. Differential scanning calorimetry (DSC) analysis was also carried out using a DSC Q2000 V24.4 (TA Instruments, USA) from room temperature to  $400 \text{ }^\circ\text{C}$  at a heating rate of  $10 \text{ }^\circ\text{C}/\text{min}$  under a nitrogen atmosphere at a flow rate of 50 mL/min. The experiment was performed by first heating, cooling, and second heating cycles.

## RESULTS AND DISCUSSION

### X-Ray Diffraction Analysis

Figure 1 shows the XRD profiles of MCC and NTC samples from various Ni-salt concentrations. All samples exhibited similar XRD patterns at diffraction peaks of  $2\theta = 15^\circ, 16^\circ, 22.8^\circ,$  and  $35^\circ$ , which can be attributed to the crystallographic planes 101, (10 $\bar{1}$ ), 021, 002, and 040, respectively (Park *et al.* 2010). This indicates that the raw material and hydrolyzed cellulose belonged to the cellulose I $\beta$  structure (French 2014). Furthermore, the main crystal structure of MCC was retained and not altered during the Ni-salt catalyzed hydrolysis process. As the concentration of Ni-salt increased from 0.05 to 1.0 M, the intensity of the XRD diffraction plane at 002 increased, becoming higher than that of MCC. This indicated an increment of crystallinity index and crystalline size of Ni-treated nanocellulose were positively affected by hydrolysis process. Based on the crystallinity profile (Table 1), the crystallinity index of samples was in the order of  $\text{MCC} < \text{NTC0.05} < \text{NTC0.5} < \text{NTC1.0}$ , showing an approximately 5% increment from that of the raw material. The increase in crystallinity index of treated samples showed a significant removal of amorphous regions and increased exposure of the crystalline regions of cellulose (Dhepe and Fukuoka 2008). As for industrial applications, crystallinity of nanocellulose is an important factor determining its mechanical and thermal properties. Higher crystallinity in nanocellulose is generally associated with higher tensile strength, which is expected to be beneficial for producing high-strength composite materials (Bhatnagar and Sain 2005).

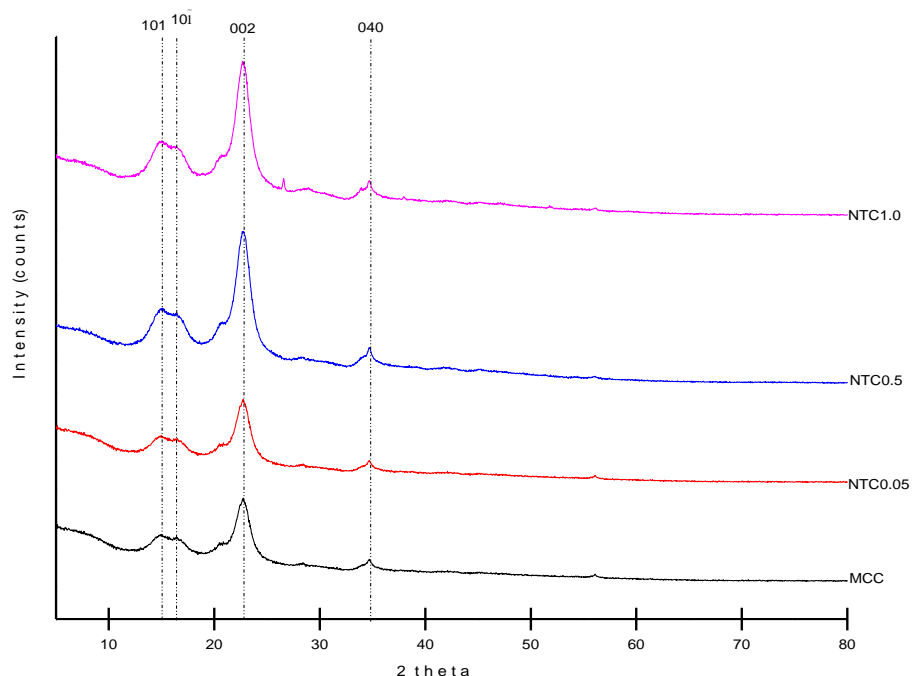


**Fig. 1.** X-ray diffraction patterns of (a) NTC1.0, (b) NTC0.5, (c) NTC0.05, and (d) MCC

As shown in Table 1, the crystallite size was increased after hydrolysis, following the order of  $MCC < NTC0.05 < NTC0.5 < NTC1.0$ . Similar cases in which the crystallite size was increased have been reported (Das *et al.* 2010; Sèbe *et al.* 2012; Shahabi-Ghahafarrokhi *et al.* 2015). It is believed that the cellulose with smaller crystallites with disorderly phases were easily degraded by high concentration of Ni-solution, which resulted in high exposure of thicker crystallite phases (Sèbe *et al.* 2012). Furthermore, the recrystallization of defective crystallites during the hydrolysis reaction may change the crystallite sizes of nanocellulose (Tang *et al.* 1996).

**Table 1.** Crystallinity Index (Crl) and Crystallite Sizes of MCC and NTCs at Various Nickel Salt Concentrations

| Sample  | $2\theta(^{\circ})$ | FWHM ( $^{\circ}$ ) | Crystallite size, D (nm)<br>(perpendicular to 200 plane) | Crystallinity index, Crl (%) |
|---------|---------------------|---------------------|--|------------------------------|
| NTC1.0  | 22.81               | 0.8600              | 9.44   | 80.75                        |
| NTC0.05 | 22.80               | 1.4196              | 5.72   | 79.82                        |
| NTC0.5  | 22.88               | 1.5807              | 5.14   | 77.84                        |
| MCC     | 22.88               | 1.7690              | 4.59   | 75.60                        |

### Fourier Transform Infrared Spectroscopy (FTIR)

The chemical functional groups of MCC, NTC0.05, NTC0.5, and NTC1.0 were studied using FTIR (Fig. 2). The four samples had similar FTIR patterns, which indicated that the chemical structure of synthesized nanocellulose remained unchanged after Ni-catalyzed hydrolysis. Furthermore, the absence of  $NO_3^-$  peaks at  $1384\text{ cm}^{-1}$  indicated that the Ni-salt was completely removed during the washing and dialysis process (Smidt *et al.* 2005; Grube *et al.* 2006).

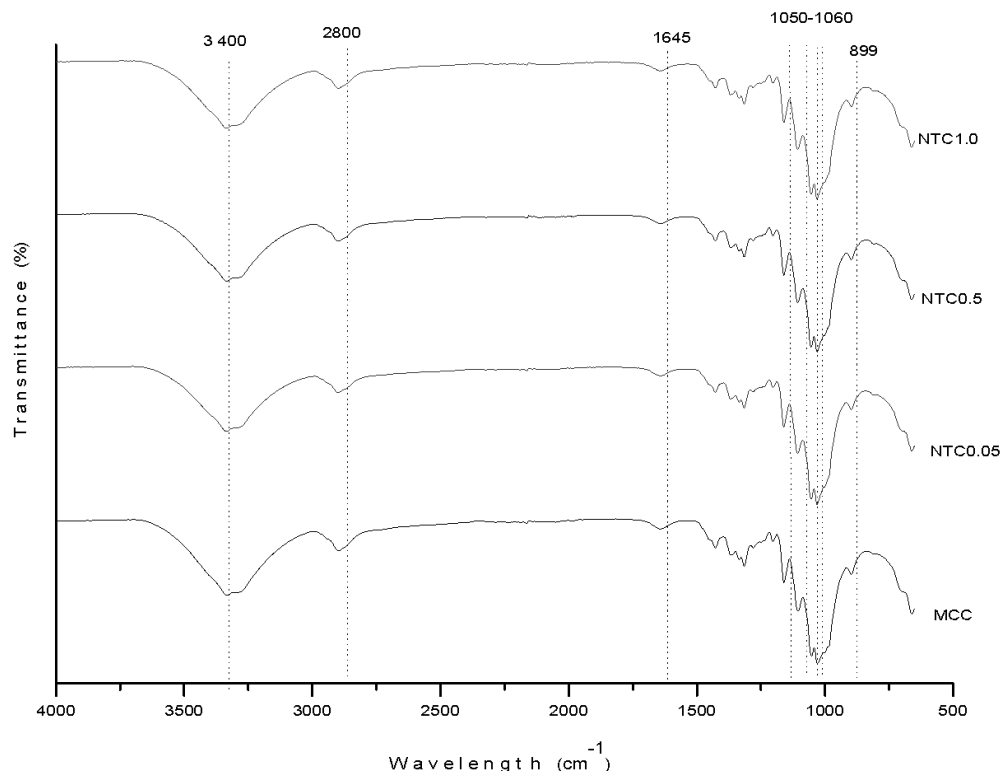


**Fig. 2.** FTIR spectra of MCC, NTC0.05, NTC0.5, and NTC1.0

The dominant peak in the region between 3700 and 3000  $\text{cm}^{-1}$  is attributed to O-H stretching. A slight decrease in the peak intensity showed the disruption of intramolecular and intermolecular hydrogen bonding (Alemdar and Sain 2008; Yang *et al.* 2011). The FTIR peak at 2,800  $\text{cm}^{-1}$  corresponds to the presence of C-H stretching vibration and  $-\text{CH}_2-(\text{C}6)-$  bending vibration (Alemdar and Sain 2008; Yang *et al.* 2011). The weak intensity of the FTIR band at 1640 to 1645  $\text{cm}^{-1}$  can be attributed to the cellulose-water interaction, *i.e.*, the  $-\text{OH}$  bending of absorbed water. The chemical structure of C-O-C pyranose ring skeletal vibration of cellulose was observed in the FTIR peak at 1,050  $\text{cm}^{-1}$  (Jahan *et al.* 2011). Furthermore, the absorption bands near 1058 to 1060  $\text{cm}^{-1}$  can be attributed to C-O and C-H stretching vibrations, which confirms the presence of cellulose structures (cellulose I as cellulose I $\beta$ ). The increasing peak intensity of these groups indicated an increase in sample crystallinity (Man *et al.* 2011; Zain *et al.* 2014). The peak at 885  $\text{cm}^{-1}$  is attributed to the characteristic  $\beta$ -glycosidic linkages between the glucose units of cellulose chains (Sun *et al.* 2004; Zhang *et al.* 2015).

### Field-Emission Scanning Electron Microscopy (FESEM)

The surface morphology of MCC and Ni-treated nanocellulose was determined using FESEM analysis (Fig. 3). At a low magnification of 100 $\times$ , MCC appeared in the form of tangled rods with ribbon like structure resembling the structure of cellulose (Das *et al.* 2010). When observed at higher magnification (20000 $\times$ ), the MCC surface consisted of a uniform compact and aggregate arrangement, where individual crystals were interconnected in an agglomerated network. FESEM images of NTC0.05, NTC0.5, and NTC1.0 are shown in Figs. 3c-f. The Ni-treated products showed the significant changes of structure as compared to MCC, where the fibers were degraded into shorter and less

orderly fragments with cracks on the surface (at low magnification). This confirmed the destruction of amorphous fraction remaining in MCC by means of mild Ni-hydrolysis, which turns the microcrystals into nanocrystals of cellulose. This finding was further supported by images with higher magnification (20000 $\times$ ) to observe the change of product surface. It was observed that the compact network of MCC was changed to spider-web-like networks with large amount of porous structures (Cao *et al.* 2013). As the Ni concentration increased, the Ni<sup>2+</sup> ions diffused into the surface of cellulose fibers and attacked the glycosidic bonding of cellulose chains. This led to the breakage of the amorphous regions of cellulose fibers, resulting in smaller particle sizes and higher fibers' porosity.

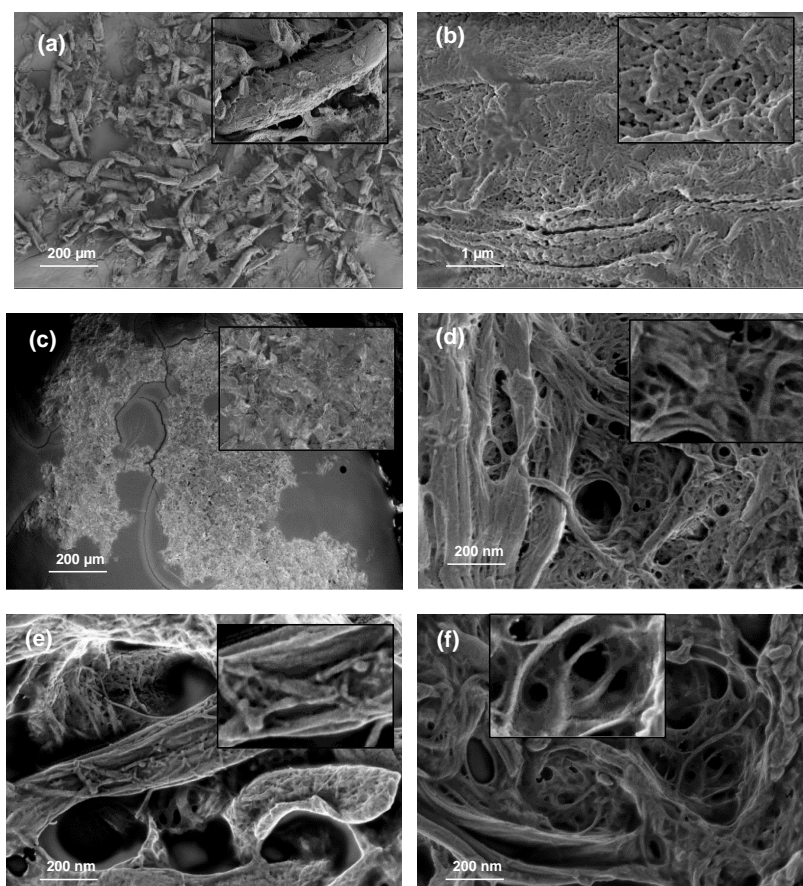


**Fig. 3.** FESEM images of (a) MCC (100 $\times$ ), (b) MCC (20000 $\times$ ), (c) NTC0.05 (100 $\times$ ), (d) NTC0.05 (20000 $\times$ ), (e) NTC0.5 (20000 $\times$ ), and (f) NTC1.0 (20000 $\times$ )

### Transmission Electron Microscopy (TEM)

TEM images of Ni-treated nanocellulose with various Ni concentrations are shown in Fig. 4. The Ni-salt-catalyzed hydrolysis rendered individual cellulose nanocrystals in porous network with spider web-like structure (Fig. 4a-c). Furthermore, the nanocellulose are presented in fine diameter (10 to 60 nm) and length at 300 to 600 nm, which implied that the Ni ion successfully diffuse into the rigid structure of MCC and resulted in selective fragmentation of crystal into smaller sizes.

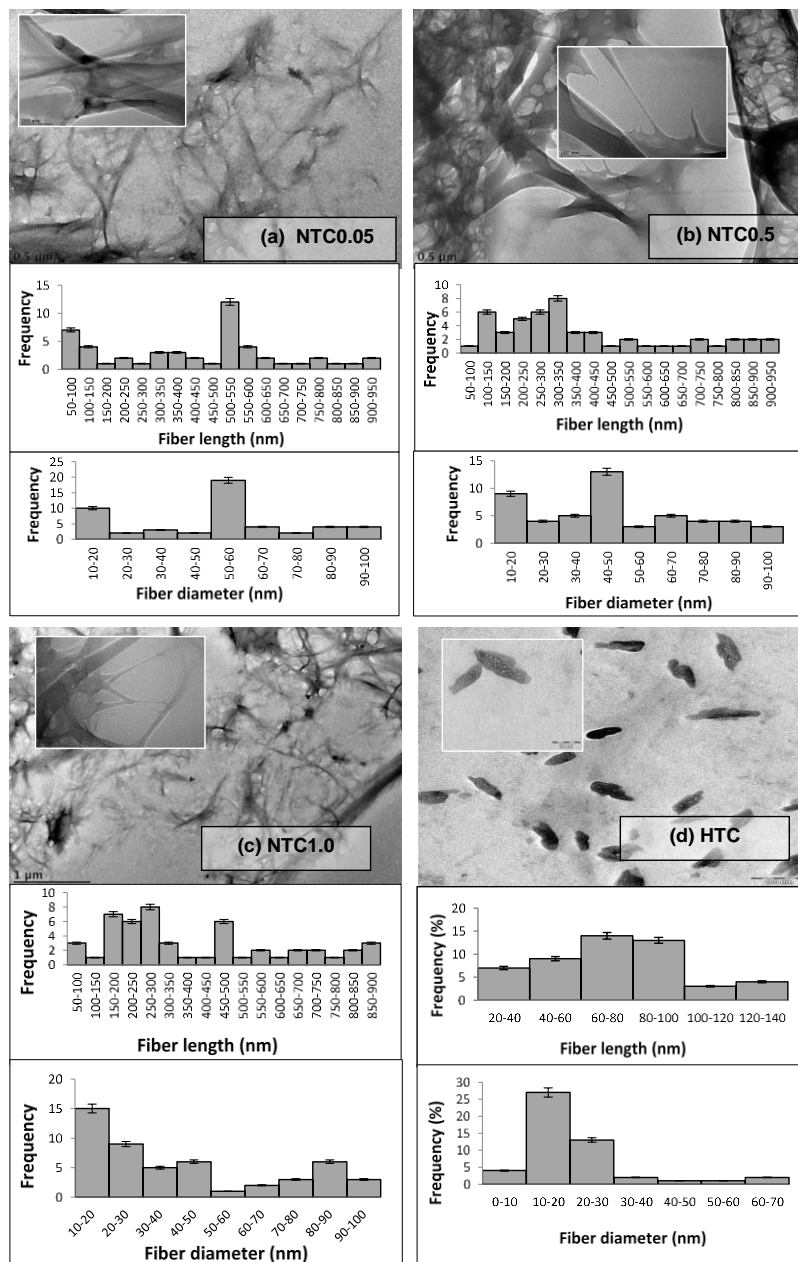


**Fig. 4.** TEM micrographs and Particle Size Distribution Profile of (a) NTC0.05, (b) NTC0.5, (c) NTC1.0, and (d) HTC

A comparison study was performed for both inorganic metal salt ( $\text{Ni}^{2+}$ ) and inorganic acid ( $\text{H}_2\text{SO}_4$ ) catalyzed hydrolysis process.  $\text{H}_2\text{SO}_4$ -treated nanocellulose (HTC) was prepared *via* hydrolysis of 40 % of  $\text{H}_2\text{SO}_4$  solution at 45 °C within 15 min (Fig. 4d). The TEM images clearly revealed the rice-shape structures of the cellulose crystals with nano-scale diameter (10 to 30 nm) and shorter length (60 to 100 nm). Besides, dimensional profiles of Ni-treated and  $\text{H}_2\text{SO}_4$ -treated nanocellulose samples were determined by studying the aspect ratio of length ( $L$ ) to diameter ( $D$ ):  $L/D$  (Table 2). The aspect ratio of prepared nanocellulose increases in the order  $\text{HTC} < \text{NTC0.05} < \text{NTC0.5} < \text{NTC1.0}$ . HTC rendered shorter length of nanocrystal while NTC showed fine width with controllable length of products. This indicated that Ni-inorganic salt capable to selectively control the

hydrolysis as compared to sulphuric acid reaction although low acid concentration was used. Among three Ni-salt concentrations, NTC1.0 rendered the most efficient mild acidity for the selective depolymerization process, where the concentration of 1.0 M is equivalent to a pH of 5.0.

**Table 2.** Dimensional Profile of Prepared Nanocellulose

| Sample   | Length (L, nm) | Diameter (D, nm) | Aspect ratio (L/D) |
|----------|----------------|------------------|--------------------|
| NTC 0.05 | 426.11±36.73   | 53.55±3.48       | 7.96               |
| NTC 0.5  | 396.02±35.26   | 47.17±3.35       | 8.40               |
| NTC 1.0  | 383.73±34.05   | 42.12±3.86       | 9.11               |
| HTC      | 72.66±1.91     | 21.51±1.91       | 3.38               |

### Thermogravimetric (TG) and Differential Thermogravimetric (DTG) Analysis

Figures 5a and b show that the thermal decomposition peaks with maximum weight loss for MCC, NTC0.05, NTC0.5, and NTC1.0 appeared at 313.21, 330.00, 331.91, and 332.74 °C, respectively. The nanocellulose product treated with the highest concentration of Ni solution (1M) had the highest thermal stability. According to the literature, the thermal stability of nanocellulose prepared by sulfuric acid hydrolysis of ionic liquids (composed of sulfate compounds) is lower than that of native cellulose (Wang *et al.* 2007; Chen *et al.* 2009; Fahma *et al.* 2010; Man *et al.* 2011). Sulfate content is thus one of the factors affecting the thermal stability of prepared nanocellulose. The presence of sulfate (residual H<sub>2</sub>SO<sub>4</sub>) adsorbed on the outer surfaces of cellulose hydroxyl crystals increases the reactivity of the material with increasing temperature, causing the decomposition of nanocellulose chains at low temperatures (Wang *et al.* 2007). In comparison, nanocellulose prepared by Ni-salt-catalyzed hydrolysis exhibits much higher thermal stability. This is due to the lesser amount of damage in the crystalline regions of cellulose structure under mild conditions. Thus, the high thermal stability of NTC1.0 means that it has many potential applications in composite materials that require high thermal stability.

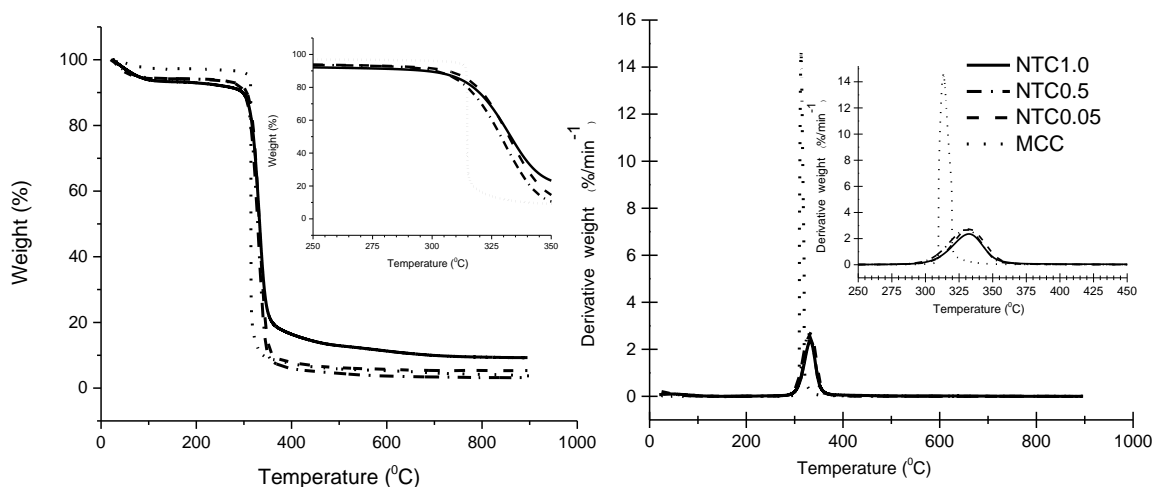


**Fig. 5.** TGA and DTG spectra for MCC, NTC0.05, NTC0.5, and NTC1.0

### Differential Scanning Calorimetry (DSC) Analysis

The thermal properties of the raw material (MCC) and prepared nanocellulose were investigated to determine the glass transition temperature ( $T_g$ ) and melting point ( $T_m$ )

through differential scanning calorimetry (DSC) analysis. Figure 6 shows sharp endothermic peaks for NTC0.05, NTC0.5, and NTC1.0, which can be attributed to the crystalline melting temperature ( $T_m$ ) of the polymer. The  $T_m$  values for NTC1.0, NTC0.5, and NTC0.05 are 154.96, 150.02, and 149.39 °C, respectively, while the  $T_m$  value for MCC is 176.90 °C. This is due to the higher molecular weight of MCC, which restricts the mobility of grafted polymer chains compared to the free polymer chains of Ni-salt treated NTC products, suggesting a higher melting transition temperature is required (Lonnberg *et al.* 2011; Dufresne 2012). Furthermore, the DSC profile shows that NTC1.0 had the highest intensity endothermic peak, which indicates that a large amount of heat at this crystalline melting temperature is required for thermal transitions in the nanocellulose polymer. This result agrees well with those regarding the thermal stability and crystallinity, where the high crystallinity of NTC1.0 gave it high thermal stability with higher heat flow for phase transitions.

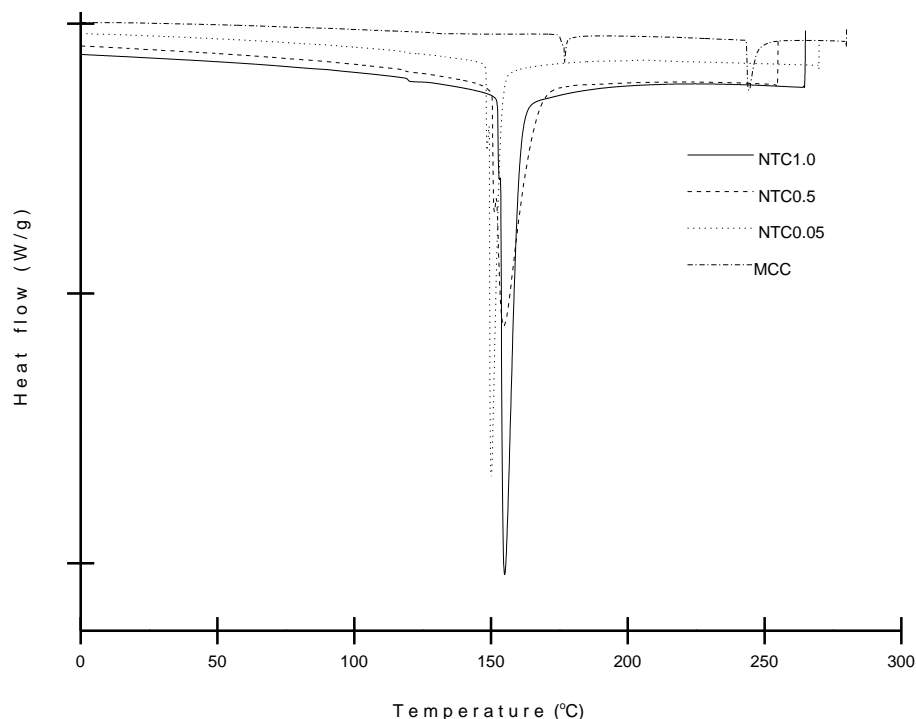


**Fig. 6.** DSC curves for NTC1.0, NTC0.5, NTC0.05, and MCC

## CONCLUSIONS

1. Nanocellulose was successfully synthesized *via* 1.0 M Ni-salt catalyzed hydrolysis of MCC.
2. Based on the XRD and FTIR analysis, there was an absence of Ni-metal and  $\text{NO}_3^-$  ions after the washing and dialysis processes of nanocellulose, which provided them with a higher thermal stability as compared to MCC.
3. The morphology of synthesized nanocellulose consisted of individual nanocrystals in web-like network with lengths ranging to several hundreds of nanometer (300 to 600 nm) and a narrow diameter distribution (10-60 nm), which means that they had a high surface area and porosity.

## ACKNOWLEDGMENTS

The authors are grateful for the financial support of the Ministry of Science, Technology and Innovation (MOSTI) e-Science Fund (grant number SF002-2015), University of Malaya, Postgraduate Research Grant Scheme PPP (PG079-2014B), and (HIR F-000032).

## REFERENCES CITED

- Alemdar, A., and Sain, M. (2008). "Isolation and characterization of nanofibers from agricultural residues – Wheat straw and soy hulls," *Bioresource Technology* 99(6), 1664-1671. DOI: 10.1016/j.biortech.2007.04.029
- Brinchi, L., Cotana, F., Fortunati, E., and Kenny, J. (2013). "Production of nanocrystalline cellulose from lignocellulosic biomass: Technology and applications," *Carbohydrate Polymers* 94(1), 154-169. DOI: 10.1016/j.carbpol.2013.01.033
- Cao, X., Wang, X., Ding, B., Yu, J., and Sun, G. (2013). "Novel spider-web-like nanoporous networks based on jute cellulose nanowhiskers," *Carbohydrate Polymers* 92(2), 2041-2047. DOI: 10.1016/j.carbpol.2012.11.085.
- Chen, Y., Liu, C., Chang, P. R., Cao, X., and Anderson, D. P. (2009). "Bionanocomposites based on pea starch and cellulose nanowhiskers hydrolyzed from pea hull fibre: Effect of hydrolysis time," *Carbohydrate Polymers* 76(4), 607-615. DOI: 10.1016/j.carbpol.2008.11.030
- Das, K., Ray, D., Bandyopadhyay, N. R., and Sengupta, S. (2010). "Study of the properties of microcrystalline cellulose particles from different renewable resources by XRD, FTIR, nanoindentation, TGA and SEM," *Journal of Polymers and the Environment* 18(3), 355-363. DOI:10.1007/s10924-010-0167-2
- Dhepe, P. L., and Fukuoka, A. (2008). "Cellulose conversion under heterogeneous catalysis," *ChemSusChem* 1(12), 969-975. DOI: 10.1002/cssc.200800129
- Dufresne, A. (2012). *Nanocellulose: From Nature to High Performance Tailored Materials*. De Gruyter, Germany.
- Fahma, F., Iwamoto, S., Hori, N., Iwata, T., and Takemura, A. (2010). "Isolation, preparation, and characterization of nanofibers from oil palm empty-fruit-bunch (OPEFB)," *Cellulose* 17(5), 977-985. DOI: 10.1007/s10570-010-9436-4
- French, A. (2014). "Idealized powder diffraction patterns for cellulose polymorphs," *Cellulose* 21(2), 885-896. DOI: 10.1007/s10570-013-0030-4
- Grube, M., Lin, J. G., Lee, P. H., and Kokorevicha, S. (2006). "Evaluation of sewage sludge-based compost by FT-IR spectroscopy," *Geoderma* 130(3-4), 324-333. DOI:10.1016/j.geoderma.2005.02.005
- Hamid, S. B. A., Chowdhury, Z. Z., and Karim, M. Z. (2014). "Catalytic extraction of microcrystalline cellulose (MCC) from *Elaeis guineensis* using central composite design (CCD)," *BioResources* 9(4), 7403-7426.
- He, J., Zhao, C., and Lercher, J. A. (2012). "Ni-catalyzed cleavage of aryl ethers in the aqueous phase," *Journal of the American Chemical Society* 134(51), 20768-20775. DOI: 10.1021/ja309915e
- Himmel, M. E., Ding, S.-Y., Johnson, D. K., Adney, W. S., Nimlos, M. R., Brady, J. W., and Foust, T. D. (2007). "Biomass recalcitrance: Engineering plants and enzymes for biofuels production," *Science* 315(5813), 804-807. DOI: 10.1126/science.1137016

- Jahan, M. S., Saeed, A., He, Z., and Ni, Y. (2011). "Jute as raw material for the preparation of microcrystalline cellulose," *Cellulose* 18(2), 451-459. DOI: 10.1007/s10570-010-9481-z
- Kamireddy, S. R., Li, J., Tucker, M., Degenstein, J., and Ji, Y. (2013). "Effects and mechanism of metal chloride salts on pretreatment and enzymatic digestibility of corn stover," *Industrial & Engineering Chemistry Research* 52(5), 1775-1782. DOI: 10.1021/ie3019609
- Karim, M. Z., Chowdhury, Z. Z., Hamid, S. B. A., and Ali, M. E. (2014). "Statistical optimization for acid hydrolysis of microcrystalline cellulose and its physiochemical characterization by using metal ion catalyst," *Materials* 7(10), 6982-6999. DOI: 10.3390/ma7106982
- Lange, J. P. (2007). "Lignocellulose conversion: An introduction to chemistry, process and economics," *Biofuels, Bioproducts and Biorefining* 1(1), 39-48. DOI: 10.1002/bbb.7
- Lee, H., Hamid, S., and Zain, S. (2014). "Conversion of lignocellulosic biomass to nanocellulose: Structure and chemical process," *The Scientific World Journal* 2014, 631013 PAGE #s. DOI: 10.1155/2014/631013
- Li, J., Zhang, X., Zhang, M., Xiu, H., and He, H. (2015). "Ultrasonic enhanced acid hydrolysis selectivity of cellulose with HCl-FeCl<sub>3</sub> as catalyst," *Carbohydrate Polymers* 117, 917-922. DOI:10.1016/j.carbpol.2014.10.028
- Lindman, B., Karlström, G., and Stigsson, L. (2010). "On the mechanism of dissolution of cellulose," *Journal of Molecular Liquids* 156(1), 76-81. DOI: 10.1016/j.molliq.2010.04.016
- Liu, L., Sun, J., Cai, C., Wang, S., Pei, H., and Zhang, J. (2009). "Corn stover pretreatment by inorganic salts and its effects on hemicellulose and cellulose degradation," *Bioresource Technology* 100(23), 5865-5871. DOI:10.1016/j.biortech.2009.06.048
- Lonnberg, H., Larsson, K., Lindstrom, T., Hult, A., and Malmstrom, E. (2011). "Synthesis of polycaprolactone-grafted microfibrillated cellulose for use in novel bionanocomposites - Influence of the graft length on the mechanical properties," *ACS Applied Material Interfaces* 3(5), 1426-1433. DOI: 10.1021/am2001828
- López-Linares, J. C., Romero, I., Moya, M., Cara, C., Ruiz, E., and Castro, E. (2013). "Pretreatment of olive tree biomass with FeCl<sub>3</sub> prior enzymatic hydrolysis," *Bioresource Technology* 128, 180-187. DOI:10.1016/j.biortech.2012.10.076
- Lu, Q., Tang, L., Lin, F., Wang, S., Chen, Y., Chen, X., and Huang, B. (2014). "Preparation and characterization of cellulose nanocrystals via ultrasonication-assisted FeCl<sub>3</sub>-catalyzed hydrolysis," *Cellulose* 21(5), 3497-3506. DOI: 10.1007/s10570-014-0376-2
- Man, Z., Muhammad, N., Sarwono, A., Bustam, M. A., Kumar, M. V., and Rafiq, S. (2011). "Preparation of cellulose nanocrystals using an ionic liquid," *Journal of Polymers and the Environment* 19(3), 726-731. DOI: 10.1007/s10924-011-0323-3
- Park, S., Baker, J. O., Himmel, M. E., Parilla, P. A., and Johnson, D. K. (2010). "Research cellulose crystallinity index: Measurement techniques and their impact on interpreting cellulase performance," *Biotechnology for Biofuels* 3(10) PAGE #s. DOI:10.1186/1754-6834-3-10
- Peng, B. L., Dhar, N., Liu, H. L., and Tam, K. C. (2011). "Chemistry and applications of nanocrystalline cellulose and its derivatives: A nanotechnology perspective," *The*

- Canadian Journal of Chemical Engineering* 89(5), 1191-1206. DOI: 10.1002/cjce.20554
- Sèbe, G., Ham-Pichavant, F., Ibarboure, E., Koffi, A. L. C., and Tingaut, P. (2012). "Supramolecular structure characterization of cellulose II nanowhiskers produced by acid hydrolysis of cellulose I substrates," *Biomacromolecules* 13(2), 570-578. DOI:10.1021/bm201777j
- Segal, L., Creely, J., Martin, A., and Conrad, C. (1959). "An empirical method for estimating the degree of crystallinity of native cellulose using the X-ray diffractometer," *Textile Research Journal* 29(10), 786-794. DOI: 10.1177/004051755902901003
- Shahabi-Ghahafarrokh, I., Khodaiyan, F., Mousavi, M., and Yousefi, H. (2015). "Preparation and characterization of nanocellulose from beer industrial residues using acid hydrolysis/ultrasound," *Fibers and Polymers* 16(3), 529-536. DOI:10.1007/s12221-015-0529-4
- Smidt, E., Eckhardt, K. U., Lechner, P., Schulten, H. R., and Leinweber, P. (2005). "Characterization of different decomposition stages of biowaste using FT-IR spectroscopy and pyrolysis-field ionization mass spectrometry," *Biodegradation* 16(1), 67-79. DOI: 10.1007/s10531-004-0430-8
- Tang, L.-G., Hon, D. N. S., Pan, S.-H., Zhu, Y.-Q., Wang, Z., and Wang, Z.-Z. (1996). "Evaluation of microcrystalline cellulose. I. Changes in ultrastructural characteristics during preliminary acid hydrolysis," *Journal of Applied Polymer Science* 59(3), 483-488. DOI:10.1002/(SICI)1097-4628(19960118)59:3<483::AID-APP13>3.0.CO;2-V
- Wang, N., Ding, E., and Cheng, R. (2007). "Thermal degradation behaviors of spherical cellulose nanocrystals with sulfate groups," *Polymer* 48(12), 3486-3493. DOI: 10.1016/j.polymer.2007.03.062
- Yang, P., Kobayashi, H., Hara, K., and Fukuoka, A. (2012). "Phase change of nickel phosphide catalysts in the conversion of cellulose into sorbitol," *ChemSusChem* 5(5), 920-926. DOI:10.1002/cssc.201100498
- Yang, Q., Pan, X., Huang, F., and Li, K. (2011). "Synthesis and characterization of cellulose fibers grafted with hyperbranched poly(3-methyl-3-oxetanemethanol)," *Cellulose* 18(6), 1611-1621. DOI: 10.1007/s10570-011-9587-y
- Zain, N., Yusop, S., and Ahmad, I. (2014). "Preparation and characterization of cellulose and nanocellulose from pomelo (*Citrus grandis*) albedo," *Journal of Nutrition & Food Sciences* 5, 334. DOI: 10.4172/2155-9600.1000334
- Zhang, Y., Li, Q., Su, J., Lin, Y., Huang, Z., Lu, Y., Sun, G., Yang, M., Huang, A., Hu, H., and Zhu, Y. (2015). "A green and efficient technology for the degradation of cellulosic materials: Structure changes and enhanced enzymatic hydrolysis of natural cellulose pretreated by synergistic interaction of mechanical activation and metal salt," *Bioresour Technol* 177, 176-181. DOI:10.1016/j.biortech.2014.11.085
- Zhao, J., Zhang, H., Zheng, R., Lin, Z., and Huang, H. (2011). "The enhancement of pretreatment and enzymatic hydrolysis of corn stover by FeSO<sub>4</sub> pretreatment," *Biochemical Engineering Journal* 56(3), 158-164. DOI: 10.1016/j.bej.2011.06.002

Article submitted: April 16, 2015; Peer review completed: August 17, 2015; Revised version received: September 17, 2015; Accepted: September 19, 2015; Published: September 24, 2015.

DOI: 10.15376/biores.10.4.7627-7639